The dual role of a multi-heme cytochrome in methanogenesis: MmcA is important for energy conservation and carbon metabolism in *Methanosarcina acetivorans*

Blake E. Downing[1], Dinesh Gupta[2], Dipti D. Nayak[2*]

Department of Plant and Microbial Biology, University of California, Berkeley, CA, USA[1];
Department of Molecular and Cell Biology, University of California, Berkeley, CA, USA[2]

Running Head: *In vivo* function of MmcA in *Methanosarcina acetivorans*

Keywords: Methane, Methanogens, *Methanosarcina*, Ferredoxin, Cytochromes

*Address correspondence to:
Dipti D. Nayak (dnayak@berkeley.edu)
Department of Molecular and Cell Biology, 1 Barker Hall #3204, University of California, Berkeley, CA 94720-3204
Tel: 510-664-5267

Abstract

Methanogenic archaea belonging to the Order *Methanosarcinales* conserve energy using an electron transport chain (ETC). In the genetically tractable strain *Methanosarcina acetivorans*, ferredoxin donates electrons to the ETC via the Rnf (**R**hodobacter **n**itrogen **f**ixation) complex. The Rnf complex in *M. acetivorans*, unlike its counterpart in Bacteria, contains a multiheme *c*-type cytochrome (MHC) subunit called MmcA. Early studies hypothesized MmcA is a critical component of Rnf, however recent work posits that the primary role of MmcA is facilitating extracellular electron transport. To explore the physiological role of MmcA, we characterized *M. acetivorans* mutants lacking either the entire Rnf complex (Δ*rnf*) or just the MmcA subunit (Δ*mmcA*). Our data show that MmcA is essential for growth during acetoclastic methanogenesis but neither Rnf nor MmcA are required for methanogenic growth on methylated compounds. On methylated compounds, the absence of MmcA alone leads to a more severe growth defect compared to a Rnf deletion likely due to different strategies for ferredoxin regeneration that arise in each strain. Transcriptomic data suggest that the Δ*mmcA* mutant might regenerate ferredoxin by upregulating the cytosolic Wood-Ljundahl pathway for acetyl-CoA synthesis, whereas the Δ*rnf* mutant may repurpose the F_{420} dehydrogenase complex (Fpo) to regenerate ferredoxin coupled to proton translocation. Beyond energy conservation, the deletion of Rnf or MmcA leads to some shared and some unique transcriptional changes in methyltransferase genes and regulatory proteins. Overall, our study provides systems-level insights into the non-overlapping roles of the Rnf bioenergetic complex and the associated MHC, MmcA.

Importance

Methane is a greenhouse gas that is ten times more potent than carbon dioxide and efforts to curb emissions are crucial to meet climate goals. Methane emissions primarily stem from the metabolic activity of microorganisms called methanogenic archaea (methanogens). The electron transport chain (ETC) in methanogens that belong to the Order *Methanosarcinales* has been the focus of many *in vitro* studies to date, but the endogenous functions of the bioenergetic complexes that comprise the ETC have rarely been investigated. In this study, we use genetic techniques to functionally characterize the Rnf bioenergetic complex and the associated multi-heme *c*-type cytochrome MmcA in the model methanogen, *Methanosarcina acetivorans*. Our results show that MmcA and Rnf have shared and unique roles in the cell, and that, contrary to current knowledge, *M. acetivorans* has the capacity to induce at least two alternative pathways for ferredoxin regeneration in the absence of a functional Rnf complex.

Introduction

The vast majority of methane released to the atmosphere is generated by a group of microorganisms called methanogens (1). Methanogens belong to the Domain Archaea and produce methane as a by-product of energy conservation (2). Methanogens are polyphyletic, and the most widely distributed mode of methanogenic growth uses molecular hydrogen to reduce carbon dioxide to methane (2, 3). Growth on hydrogen and carbon dioxide (termed hydrogenotrophic methanogenesis) is a highly conserved and well-characterized seven-step pathway (Supplementary Figure 1a) (3). A few methanogens, notably members of the Order *Methanosarcinales,* have an expanded metabolic repertoire that includes growth on small organic acids like acetate (via acetoclastic methanogenesis) or on methylated compounds like methanol or methylamines (via methylotrophic methanogenesis) (Supplementary Figure 1b-1e) (2, 4). The metabolic versatility of the *Methanosarcinales* is linked to the presence of a membrane-bound electron transport chain (ETC) for energy conservation, which is absent in many other methanogen lineages (2, 4).

In the *Methanosarcinales*, the ETC can be broken down into one or more input modules, a membrane-bound electron carrier called methanophenazine (MP), and a single output module (4, 5). The input module(s) serve as an entry point for electrons from a variety of electron donors and cofactors into the ETC whereas the output module transfers electrons to the terminal electron acceptor (4). Depending on the strain and the growth substrate, the input module(s) can vary substantially but the output module remains constant because the terminal electron acceptor is always a heterodisulfide (CoM-S-S-CoB) of two cofactors, coenzyme M (CoM) and coenzyme B (CoB) (Figure 1) (3, 4, 6). The CoM-S-S-CoB is generated by the enzyme methyl coenzyme M reductase (MCR) in the last step of methanogenesis (Supplementary Figure 1) (3, 6).

Accordingly, all members of the *Methanosarcinales* encode a membrane-associated heterodisulfide reductase complex (HdrDE) that serves as the output module of the ETC (4, 7, 8). HdrDE transfers electrons from reduced MP to CoM-S-S-CoB, regenerating coenzyme M (CoM-SH) and coenzyme B (CoB-SH) (Figure 1) (7, 9). Concomitantly, oxidation of MP by HdrDE releases two protons to the pseudoperiplasmic space via a redox loop mechanism (9). In contrast to the omnipresent HdrDE, the input module(s) of the ETC are diverse and, while resembling many of their bacterial counterparts, these bioenergetic complexes have many unique features whose functional ramifications remain poorly characterized.

Within the Genus *Methanosarcina*, strains derived from freshwater environments like *M. barkeri* Fusaro rely on hydrogenases for energy conservation via a process termed "hydrogen cycling" (4, 10–12). However, the marine methanogen *Methanosarcina acetivorans* does not produce any active hydrogenases, and therefore does not rely on hydrogen cycling for the generation of an ion motive force (11, 13). Instead, *M. acetivorans* transfers electrons from reduced cofactors directly to MP via two dedicated bioenergetic complexes: the F_{420} dehydrogenase complex (Fpo) and the *Rhodobacter* nitrogen fixation complex (Rnf) (Figure 1a) (4, 14, 15). The Fpo complex couples the transfer of electrons between the cytosolic F_{420} pool and the membrane-bound MP pool to the translocation of protons across the membrane (Figure 1a) (4, 16). The Fpo complex is related to Respiratory Complex I (RCI) in the mitochondria of eukaryotes and the NADH:ubiquionine oxidoreductase (Nuo) from bacteria, except the NADH interacting module NuoEFG is replaced by the non-orthologous module FpoF (16, 17). In comparison, the Rnf complex couples the transfer of electrons between ferredoxin and MP to the translocation of sodium ions across the membrane (Figure 1a) (15, 18, 19). The genetic

organization and cellular function of the Rnf complex in methanogens differs substantially from its bacterial counterparts.

In Bacteria, the Rnf complex is composed of six subunits: RnfABCDEG, and preliminary evidence indicates that electrons flow from reduced Fd to the iron-sulfur clusters of RnfB, then to the covalently bound flavin mononucleotide (FMN) cofactors of RnfG and RnfD, and finally to NAD^+ in the cytosol via the iron-sulfur clusters of RnfC (Figure 1c) (20). However, no structure has been solved for the complex, so additional cofactors involved in electron flow may be present (20, 21). In addition to the core subunits described above, the *rnf* operon of methanogens also contains an additional gene that encodes a multi-heme *c*-type cytochrome (MHC), *mmcA* (Figure 1d) (18, 22). While the known redox cofactor binding sites of RnfB, RnfD, RnfG and RnfC are conserved in *M. acetivorans,* whether the flow of electrons from Fd from MP follows the same pathway hypothesized in bacterial systems, and how MmcA is involved in this process remains unclear (18, 19). Recent evidence indicates that MmcA in *M. acetivorans* might instead act as a conduit for extracellular electron transfer (EET) to external electron acceptors like anthraquinone-2,6-disulfonate (AQDS), which would substantially broaden the metabolic repertoire of *M. acetivorans* beyond methanogenic growth (22). While it is abundantly clear that MmcA plays an important role in the energy metabolism of *M. acetivorans* and other members of the *Methanosarcinales,* the underlying mechanism(s) remains poorly characterized.

In this study, we use a genetic approach to elucidate the *in vivo* function of MmcA in the model methanogen *M. acetivorans* by comparing the growth and transcriptional responses of mutant strains lacking the MmcA subunit or the entire Rnf complex. Our results show that MmcA might have a cellular function beyond facilitating electron flow through the Rnf complex.

Our transcriptomic data also shed light on the coupling between substrate-specific methyltransferases and energy conservation pathways in *M. acetivorans* and bring to light alternate routes for the regeneration of reduced ferredoxin in the absence of Rnf. Overall, our work underscores the importance of MmcA in the methanogen Rnf complex and elucidates a broader role for this multiheme cytochrome during methanogenesis.

Results and Discussion

Validation of mutant strains lacking *mmcA* or *rnf* in *Methanosarcina acetivorans*

The *rnf* locus in *M. acetivorans* consists of eight ORFs (MA0658 to MA0665) that encode MmcA and RnfCDGEABX respectively (Figure 2a). The first seven genes have overlapping coding regions and previous studies have also shown that all eight genes are transcribed in a single operon (Figure 2a) (18). To characterize the *in vivo* function of the Rnf complex, we obtained a mutant that has a markerless in-frame deletion in the *M. acetivorans* chromosome spanning *mmcA* through *rnfX* as described in (23) (Figure 2b). To understand the function of the MmcA gene in the Rnf complex, we generated a markerless in-frame deletion in the *mmcA* gene as described previously using Cas9-mediated genome editing (24, 25) (Figure 2c). We sequenced the genome of the Δ*mmcA* mutant and, relative to the parent strain (WWM60), did not detect mutations elsewhere on the chromosome (Supplementary Table 1). Based on this evidence, we can conclude that our MmcA deletion strain does not have any off-target mutations as a result of Cas9 editing or any suppressor mutations to compensate for the loss of *mmcA*.

Since *mmcA* is the first gene in the *rnf* operon, it is likely that deletion of *mmcA* could alter the expression of the other *rnf* genes. To test for polar effects, we measured the expression of *rnfCDGEABX* in the Δ*mmcA* mutant and WWM60 using whole-genome RNA sequencing

during growth on trimethylamine (TMA) and did not detect significant change in transcript levels of any of these genes in the absence of *mmcA* (p-value >0.05; Welch's t-test) (Figure 1d). Thus, knocking out the *mmcA* gene does not alter the transcription of *rnfCDGEABX*. In addition, we observed that expression of *mmcA in trans* functionally complements the chromosomal deletion of *mmcA* and restores wildtype growth on TMA (Figure 2e). These growth data indicate that the RnfCDGEABX proteins are produced in the Δ*mmcA* mutant and that expression of *mmcA* in *trans* can reconstitute a functional Rnf complex.

Growth characteristics of *rnf* and *mmcA* mutants during methanogenesis on different substrates

In vitro analyses of the Rnf complex from *M. acetivorans* suggest that MmcA plays an important role in mediating electron flow between ferredoxin and MP, but the importance of MmcA for Rnf activity *in vivo*, outside of extracellular electron transfer, has not been well characterized (22). To address this gap in knowledge, we measured the growth phenotype of WWM60, Δ*rnf*, and Δ*mmcA* on a wide range of substrates that represent the metabolic breath of *M. acetivorans.*

The Rnf complex as well as MmcA are essential for growth on acetate via acetoclastic methanogenesis (18, 23, 24). We observed no growth of the Δ*rnf* or Δ*mmcA* mutants on acetate, while WWM60 with a fully functional Rnf complex was viable (Figure 3a, Table 1). We attempted to isolate suppressor mutants in the Δ*rnf* or Δ*mmcA* backgrounds that restore growth on acetate by incubating each strain in growth medium containing acetate as the sole source of carbon and energy. We did not detect any observable growth (measured as a change in optical density) for all three replicates of either strain after an incubation period of one year. Together, these results indicate that the Rnf complex is essential during methanogenesis from acetate for

regenerating reduced ferredoxin generated by the carbon monoxide dehydrogenase/acetyl CoA synthase (CODH/ACS) complex (18, 26, 27). In addition, the MHC subunit MmcA is vital for the functionality of the Rnf complex. Our growth data for the Δ*mmcA* mutant on acetate agree with previous work from our group, but are in contrast a previous study where a *mmcA* deletion mutant of *M. acetivorans* had no growth defect on acetate compared to the corresponding parent strain (22, 24). We suspect that the difference in phenotype observed may pertain to differences in the genetic techniques used for generating deletion mutants, or the presence of a suppressor mutation in the *mmcA* deletion strain generated in the previous work (22).

Next, we tested the role of Rnf and MmcA during methylotrophic methanogenesis by measuring the growth phenotype of the mutants and the parent strain on three different methylated compounds: trimethylamine (TMA), methanol (MeOH), and dimethylsulfide (DMS) (14, 28–30). The Δ*rnf* mutant and the Δ*mmcA* mutant were viable on all three methylated compounds, but we noted a significant defect in the growth rate of both mutants relative to WWM60 (Figure 3b, Table 1). Additionally, the Δ*mmcA* mutant had a significantly higher growth defect compared to the Δ*rnf* mutant on all methylated compounds (Figure 3; Table 1). Based on these data, we can conclude that tMmcA and other components of the Rnf complex are not essential for methylotrophic methanogenesis in *M. acetivorans* but are important for optimal growth under these conditions.

The phenotypes of the Δ*rnf* and Δ*mmcA* strains also differed when switching between methylotrophic substrates. We observed that the Δ*rnf* mutant had a significantly shorter lag time switching from medium containing TMA to medium with DMS relative to both WWM60 and the Δ*mmcA* mutant (Figure 4a; Table 2). The lag time of the Δ*mmcA* mutant is not significantly different from the WT strain (Figure 4a; Table 2), further supporting the hypothesis that Rnf

proteins are expressed in the absence of MmcA during methylotrophic growth. Based on these data, we hypothesize that loss of the Rnf complex, but not MmcA alone, might result in a transcriptional response tuning the expression of methyltransferases (such as *mtsD*, *mtsF,* and *mtsH*) that are required for growth on methylated sulfur compounds like DMS (30). However, the sensory and regulatory pathway(s) by which this transcriptional response is carried out cannot be inferred from these data.

As the growth defect for the Δ*mmcA* mutant on methylated compounds was significantly exacerbated compared to the Δ*rnf* mutant (Figure 3), it is likely that, in addition to being an important part of the Rnf complex in methanogens, MmcA may have other physiological roles too. To test for a Rnf-independent function of MmcA during methylotrophic methanogenesis, we generated a strain encoding the *mmcA* gene on a plasmid in the Δ*rnf* background (Figure 4b) and measured the growth of this mutant on TMA relative to a control strain carrying an empty vector. Indeed, expression of *mmcA* in the Δ*rnf* background enhanced growth rate compared to the control strain by 22% [p-value = 0.0023; Welch's t-test] (Figure 4b and Supplementary Table 2). Growth yield of the Δ*rnf* strain expressing *mmcA* was not significantly different than the control strain (Supplementary Table 2). These phenotypic data provide clear evidence that the physiological role of MmcA during methanogenesis from methylated compounds extends beyond its capacity to relaying electrons through the Rnf complex.

Differential expression of Fpo and methylamine methyltransferases lead to differential growth of the Δ*rnf* and Δ*mmcA* mutants

Based on our growth data, it is clear that the cellular function of the Rnf complex does not completely overlap with the MHC subunit, MmcA, during methylotrophic growth. To understand the genetic basis for this phenotypic distinction, we performed whole genome RNA

sequencing of the Δ*rnf* mutant, the Δ*mmcA* mutant and WWM60 at mid-exponential growth on TMA. To identify genes that are "differentially expressed", we used the following the criteria: a $\log_2$-fold change in transcript abundance ≥2 (4-fold) with a q-value (corrected p-value) ≤0.01 (see Materials and Methods). The Δ*rnf* mutant had significantly higher expression of genes involved in two distinct aspects of methanogenic metabolism relative to the Δ*mmcA* mutant (Figure 5a). First, we observed significantly higher transcripts for several genes encoding the F_{420} methanophenazine oxidoreductase (Fpo) bioenergetic complex. The membrane bound Fpo complex is comprised of thirteen subunits and, during methylotrophic growth, catalyzes the transfer of electrons from reduced F_{420} to MP coupled to the translocation of two protons across the membrane (Figure 1) (16). Most of the genes comprising the Fpo complex are encoded in the *fpoABCDHIJ1J2KLMNO* operon (Figure 5b) (16, 31). The F_{420} input module *fpoF* is found elsewhere on the chromosome in putative operon with the F_{420}-dependent N(5),N(10) -methylene tetrahydromethanopterin reductase (*mer*), and a second copy of *fpoO2* is encoded close to the *fpoA-O* operon, although neither paralog has a known function (Figure 5b) (31). Five genes in the *fpo* operon (*fpoJ2, fpoL, fpoM, fpoN,* and *fpoO*) as well as *fpoO2* had ≥4-fold (or 2 $\log_2$-fold) higher expression in the Δ*rnf* background compared to the Δ*mmcA* mutant (Figure 5b; Supplementary Table 3). No significant change in expression was observed for *fpoF* (Supplementary Table 3). Thus, we hypothesize that a "headless" or modified form of Fpo that lacks the F_{420} interacting module FpoF is more abundant in the Δ*rnf* mutant. The "headless" Fpo complex has been hypothesized to function as a ferredoxin: MP oxidoreductase in other methanogens, like members of the Genus *Methanothrix (*previously known as Genus *Methanosaeta*) that lack both the Ech hydrogenase as well as the Rnf complex (32). While previous studies have suggested that FpoO plays a role in transferring electrons from the Fpo

complex to the MP pool via a [2Fe-2S] cluster, we hypothesize that the FpoO subunit might instead interact with the FpoF subunit and/or with ferredoxin directly (31). It is possible that the two copies of FpoO encoded in the *M. acetivorans* genome differ in their affinity for FpoF versus ferredoxin, which might further modulate the specificity of the Fpo complex for different electron carriers. Altogether, we postulate that higher expression of other subunits of the Fpo complex relative to FpoF and tuning the amount of FpoO2 relative to FpoO1 increases the proportion of the "headless" Fpo complex in the Δ*rnf* mutant (Supplementary Figure 2). The "headless" Fpo complex might provide an alternate route for ferredoxin regeneration in the Δ*rnf* mutant that ultimately leads to faster growth under methylotrophic conditions compared to the Δ*mmcA* mutant. The RNA sequencing data do not allow us to discriminate whether the Fpo genes are upregulated in the Δ*rnf* mutant or downregulated in the Δ*mmcA* mutant. To distinguish between these two modes of regulation, we compared the expression of the Fpo locus in each mutant relative to WWM60. The Fpo genes were more highly expressed in the Δ*rnf* mutant, but not in the Δ*mmcA* mutant, compared to WWM60, however the change in expression for both mutants did not meet our ≥2 $\log_2$-fold threshold value. Thus, our data suggest the loss of Rnf might result in upregulation of Fpo (Supplementary Table 3), but we cannot confidently identify a mode of regulation that causes a differential expression of the Fpo genes in the Δ*rnf* strain relative to the Δ*mmcA* strain at present.

In addition to the Fpo genes, we also observed significantly higher expression of multiple genetic loci that encode TMA, DMA (dimethylamine), and MMA (monomethylamine) methylamine methyltransferases as well as permeases putatively involved in the transport of these methylated amines in the Δ*rnf* mutant relative to the Δ*mmcA* mutant (Figure 5a, 5c; Supplementary Table 4) (33, 34). Differential expression of these genes could lead to a

commensurate change in the rate of transport and conversion of methylated amines to methyl-coenzyme M, an intermediate that feeds into the core methanogenic pathway, which ultimately would affect cell growth as observed in Figure 3. To determine if transcription of these loci was induced in the Δ*rnf* mutant or restricted in the Δ*mmcA* mutant, we compared the expression of these genes in each mutant relative to WWM60 independently. While we did not detect any significant change in transcript levels of any of these genes in the Δ*rnf* mutant relative to WWM60, whereas most of these genes had 4 to 5-fold higher expression in WWM60 relative to the Δ*mmcA* mutant (Supplementary Table 4). These data strongly suggest that the methyltransferase loci are downregulated only when the *mmcA* locus is deleted but not when the entire the entire *rnf* locus is deleted. While the mechanistic details of this regulatory process are beyond the scope of this work, these data bring to light previously unknown global mechanisms in methanogens that coordinate the expression of genes involved in energy conservation (such as *mmcA* and *rnf)* with genes involved in carbon metabolism (such as the *mttCB, mtbCB, mtmCB* methyltransferases involved in growth on TMA, DMA, and MMA, respectively) (33, 34).

Nearly forty genes had significantly higher expression in the Δ*mmcA* mutant relative to the Δ*rnf* mutant and these could be divided into three categories: a) genes that were globally upregulated in the Δ*mmcA* mutant, i.e. these genes were also expressed to a higher level in the Δ*mmcA* mutant relative to WWM60, b) genes that were globally downregulated in the Δ*rnf* mutant i.e. genes that also had a lower expression in the Δ*rnf* mutant compared to WWM60, and c) genes that were only expressed to a higher degree in the Δ*mmcA* mutant relative to the Δ*rnf* mutant, i.e. genes that were not differentially expressed when comparing either mutant to WWM60 (Supplementary Table 5). Of the six genes in the first category, four lacked any

recognizable motifs or domains and the other two encode proteins involved in the biosynthesis of asparagine (*asnB*) and post-translational modification of proteins (O-linked N-acetylglucosamine transferase) (Supplementary Table 5) (35, 36). At present, a connection between MmcA and these proteins remains elusive.

About twenty genes were consistently downregulated in the Δ*rnf* mutant and this list includes *rnfCDGEABX* (which validates our methods for identifying changes in transcription), biosynthetic genes, and several genes likely involved in transcriptional regulation (Supplementary Table 5). Downregulated biosynthetic genes included *thiC* (MA4010), a UbiA prenyltransferase domain containing protein, which catalyzes the synthesis of lipophilic compounds that serve as electron carriers in the ETC (37, 38). We hypothesize *ubiA* is involved in the biosynthesis of MP and, in the absence of Rnf, transcription is reduced to modulate levels of MP in the membrane. This hypothesis agrees with a previous study where *ubiA* and other predicted ubiquinone/menaquinone biosynthetic genes were proposed to be involved in MP synthesis and more highly expressed in *M. barkeri* during direct interspecies electron transfer (DIET) to facilitate extracellular electron transport through the membrane (38). Other downregulated biosynthetic genes included a putative operon with an acyl carrier protein and a long chain fatty acyl CoA ligase (MA1027-MA1029). We also observed downregulation of several regulatory genes included an ArsR family transcriptional regulator (MA0504), a response regulator (MA4671), as well as a protein with a DNA-binding helix-turn-helix motif (MA4484) (Supplementary Table 5). The targets of the various regulatory proteins are unknown but might be one of biosynthetic genes mentioned above or the DMS specific methyltransferases, based on the shortened lag time observed in Figure 3d.

Finally, a set of thirteen genes had higher expression only in the Δ*mmcA* mutant relative to the Δ*rnf* strain but were not differentially expressed in comparison to WWM60 (Supplementary Table 5). This list includes signaling proteins like a sensory transduction histidine kinase (MA2256), regulatory genes such as *nikR*, a nickel-responsive transcriptional regulator that controls the expression of nickel-containing enzymes, and cofactor biosynthetic genes like *nadE,* which encodes NAD synthetase that catalyzes the last step in NAD biosynthesis (39, 40). It is tempting to speculate that the signaling proteins or the regulators identified above are linked to the downregulation of the methylamine specific methyltransferases in the Δ*mmcA* strain (Figure 5c; Supplementary Table 4), however detailed mechanistic analyses would be needed to bolster this observation in future work.

Overall, our RNA-sequencing analyses provided clear insights into the genetic basis of the phenotypic distinctions between the Δ*mmcA* strain and the Δ*rnf* strain observed in Figure 3. Downregulation of substrate specific methyltransferases and lower levels of the "headless" Fpo complex, which can potentially regenerate reduced ferredoxin, leads to a more severe growth defect for the Δ*mmcA* mutant relative to the Δ*rnf* mutant on methylated substrates.

Novel routes for generating a Na^+ ion gradient and regenerating ferredoxin enable methylotrophic growth in the absence of a functional Rnf complex

To understand how the Δ*rnf* and Δ*mmcA* mutants sustain growth on methylated compounds and the physiological basis for the fitness defect they incur (Figure 3), we compared the transcriptomic profile of each mutant in mid-exponential phase on TMA to that of WWM60 under the same growth conditions (Figure 6a and Figure 6b). Genes were classified as being "differentially expressed" if they met the same criteria listed above. The expression level of

genes in WWM60 was considered to be the baseline, so genes with significantly higher or lower transcript levels in the mutants were considered to be upregulated or downregulated respectively.

Only thirteen genes were upregulated and twenty-four genes were downregulated in both mutants compared to WWM60 (Supplementary Table 6). The upregulated genes belonged to three distinct gene clusters (Figure 6a and Figure 6b). First, with the exception of *pstS,* all other genes of the high-affinity phosphate (Pi) transport system (*pstSCAB-phoU)* and alkaline phosphatase (*phoA*) were upregulated between 4.0 to 12-fold in the mutants (Supplementary Table 6) (41). Previous studies with *M. mazei* have shown that cells experiencing Pi starvation upregulate *pstSCAB-phoU* as well as *phoA* (41). Here, we anticipate that these mutants have upregulated the phosphate transport and hydrolysis genes to meet an increased cellular demand for Pi despite slower growth. We suspect that the excess Pi might be needed for ATP synthesis or biosynthesis of methanogenic cofactors, such as tetrahydrosarcinopterin (H_4SPT) and coenzyme B. The *M. acetivorans* genome also encodes a low-affinity Pi transport system (MA2934-MA2935) that was not differentially expressed in these strains (Supplementary Table 7) (42). Next, several genes in the operon encoding the F_1F_O ATP synthase were upregulated by 4.0 to 8.0-fold in both mutants (Figure 6c; Supplementary Table 6). *M. acetivorans* encodes two different ATP synthases: an archaeal A_1A_O ATP synthase (MA4152-MA4160), which can translocate H^+ ions and Na^+ ions concomitantly, that is essential for growth (43), as well as a bacterial F_1F_O ATP synthase (MA2433-MA2441) that is dispensable during methylotrophic methanogenesis and is hypothesized to only translocate Na^+ ions (44). During methylotrophic growth, the Rnf complex generates a Na^+ gradient that is used for: a) ATP synthesis by the promiscuous A_1A_O ATP synthase and b) the endergonic transfer of the methyl group from methyl-CoM to H_4SPT catalyzed by N^5-methyl-H_4SPT (CH_3-H_4SPT): Coenzyme M (CoM)

353 methyltransferase (Mtr) (Supplemental Figure 1) (3, 43). In the absence of a functional Rnf
354 complex, we hypothesize that the A_1A_O ATP synthase relies solely on the proton gradient
355 generated by Fpo and HdrDE for ATP synthesis and the F_1F_O ATP synthase is upregulated to
356 generate a Na^+ gradient via ATP hydrolysis, which can then be used for the endergonic reaction
357 catalyzed by Mtr. Our hypothesis is further corroborated by the observation that the upregulated
358 genes in the F_1F_O ATP synthase locus are either involved in the assembly of the membrane-
359 embedded F_O domain (*atpI*; MA2439) or encode the 'a' subunit (*atpB*; MA2437) and the 'c' ring
360 (*atpE*; MA2436) of the F_O complex that bind and translocate Na^+ ions (44, 45). In a previous
361 study, a multi-subunit Na^+/H^+ antiporter (encoded by the Mrp locus) was shown to play an
362 important role in coupling growth and methanogenesis by generating an optimal Na^+/H^+ gradient
363 for efficient ATP synthesis on acetate (46). We did not observe a significant change in the
364 expression of the Mrp locus in either mutant (Supplementary Table 7). Thus, the putative role of
365 the F_OF_1 synthase in generating a Na^+ gradient in the Δ*rnf* and the Δ*mmcA* mutants is non-
366 overlapping with the cellular function of Mrp and other Na^+/H^+ antiporters, and potentially
367 highlights different strategies for balancing ion gradients depending on the methanogenic
368 substrate. Finally, the *mtpCAP* locus was upregulated by 8 to 11-fold in the Δ*rnf* mutant and by
369 16 to 22-fold in the Δ*mmcA* mutant (Supplementary Table 6). Recent studies have shown that the
370 *mtpCAP* locus is involved in the transport and catabolism of the methylated sulfur compound
371 methylmercaptopropionate (MMPA) in *M. acetivorans* (47), however no MMPA was present in
372 our growth media. At present, neither the cause for upregulation of the *mtpCAP*
373 methyltransferase system nor its effect on the physiology of the mutants is clear. However, this
374 observation demonstrates the intricate coupling between methyltransferase regulation and energy
375 conservation in methanogens. Genes that are downregulated in the two mutants have core

376 housekeeping functions and we anticipate that the differential expression of these loci is a
377 consequence of slower growth in the mutants (Supplementary Table 6).

378 Next, we analyzed the subset of genes that were differentially expressed in only one of
379 the two mutants. In the Δ*rnf* mutant, three genes were upregulated and ten genes were
380 downregulated in comparison to WWM60 (Supplementary Table 8). Oddly, the *hypF* gene
381 involved in the maturation of hydrogenases (48) was upregulated 6.5-fold, even though *M.*
382 *acetivorans* lacks any detectable hydrogenase activity during methylotrophic growth conditions
383 (13). In addition, the *kefC* locus encoding a putative glutathione regulated K^+ efflux system was
384 also upregulated 4-fold in the Δ*rnf* mutant. KefC has been shown to transport Li^+ and Na^+ ions
385 (49), therefore we hypothesize that this locus might also aid in establishing a Na^+ ion gradient in
386 the absence of Rnf. Apart from some genes encoding the pseudo periplasmic substrate binding
387 protein of various ABC transporters, the majority of genes uniquely downregulated in the Δ*rnf*
388 mutant compared to WWM60 did not have a recognizable functional motif (Supplementary
389 Table 8).

390 In contrast to the Δ*rnf* mutant, a substantially larger number of genes are uniquely
391 induced or suppressed in the Δ*mmcA* mutant (Supplementary Table 9). Among the genes that are
392 upregulated, a few loci are particularly notable. First, genes encoding the carbon monoxide
393 dehydrogenase/acetyl CoA synthase (CODH/ACS) enzyme are upregulated by 4.0 to 7.0-fold.
394 *M. acetivorans* contains two isoforms of CODH/ACS that are encoded by the *cdh1* and *cdh2*
395 operons (Figure 6d) (50). Our initial analysis indicated that five subunits of *cdh1* (*cdhA1*, *cdhB1*,
396 *cdhC1*, *cooC1*, and *cdhD1*) and three subunits of *cdh2* (*cdhC2*, *cooC2*, *cdhD2*) are upregulated in
397 the Δ*mmcA* mutant. Upon closer inspection, we noticed that the two *cdhA* and *cdhB* homologs
398 are relatively divergent at the sequence level (~80% amino acid identity) whereas the *cdhC*,

399 *cooC*, *cdhD* homologs share >97% amino acid identity (14). Thus, the upregulation of the latter
400 set in *cdh2* could be an artefact of the RNA-sequencing analysis pipeline, similar to previous
401 reports of transcript cross-reactivity between *cdh* operons in *M. mazei* (51). Regardless, both
402 isoforms are known to be functionally redundant and can catalyze the catabolism of acetate
403 during acetoclastic methanogenesis or anabolic acetyl-CoA synthesis by the Wood-Ljundahl
404 (WL) pathway during methylotrophic growth (50). Since carbon fixation by the WL pathway
405 requires reduced ferredoxin, increased expression of CODH/ACS could serve as an alternate
406 route for regenerating reduced ferredoxin in the absence of a functional Rnf complex in the
407 Δ*mmcA* mutant. A 4.0-fold increase in expression of the regulatory protein encoded by the *mreA*
408 locus in the Δ*mmcA* mutant is likely linked to the upregulation of *cdh1*. MreA is a global
409 regulator of methanogenic pathways in *M. acetivorans* and has been shown to activate genes
410 important for acetoclastic methanogenesis (such as *cdh1*) and to repress transcription of genes
411 that play a crucial role in methylotrophic methanogenesis (including the methylamine-specific
412 methyltransferases and the *fpo* locus) (Figure 5b and Figure 5c) (52). In a previous study, the
413 *ack/pta* locus encoding acetate kinase and phosphate acetyltransferase were downregulated in a
414 Δ*mreA* strain, however we did not observe any significant change in the expression of these loci
415 in the Δ*mmcA* mutant (Supplementary Table 7) (52). Thus, it is likely that other regulators in
416 addition to MreA are also involved in the upregulation of genes required for the catabolism of
417 acetate. We also observed a 5.6-fold increase in expression of a gene encoding a bile acid: Na^+
418 symporter family protein (MA2632) in the Δ*mmcA* mutant, which may be linked to the
419 maintenance of the Na^+ ion gradient across the membrane. Among the genes that were
420 significantly downregulated in the Δ*mmcA* mutant, two loci are of particular interest. First, the
421 *pylBCD* locus involved the biosynthesis of the 22nd amino acid, pyrrolysine (Pyl), is

downregulated by 4.0 to 4.6-fold (53). Whether the *pyl* genes are a part of the same regulon as the concomitantly downregulated methylamine methyltransferases (Figure 5c) or if the expression of the *pyl* genes is controlled by the amount of the methylamine methyltransferases remains unclear. Next, two genes (*cfbA* and *cfbE)* involved in the biosynthesis of Factor 430 (F_{430}), a Ni-containing cofactor associated with MCR, were downregulated significantly (54, 55). Downregulation of F_{430} production might free up more Ni for increased production of the Ni-containing CODH/ACS enzyme in Δ*mmcA* mutant.

Conclusions

The acquisition of an ETC likely spurred rampant ecological diversification in members of the Order *Methanosarcinales.* For several decades, the bioenergetic complexes that comprise the ETC in these archaea were studied in isolation using *in vitro* techniques. While these studies have provided substantial insights into the biochemical mechanisms that facilitate electron transfer reactions, an *in vivo* perspective on the ETC and its interplay with metabolism has been lacking. In this study, we performed comprehensive genetic, phenotypic, and transcriptomic analyses of *M. acetivorans* mutants that either lack the entire Rnf bioenergetic complex or a just a single subunit encoding an MHC called MmcA. Our growth analyses are congruent with a previous study, which also demonstrated that Rnf complex is essential for growth on acetate but not on methylated compounds (15). Our transcriptomic analyses provide evidence of potential alternative mechanisms for ferredoxin regeneration in each mutant (Figure 5b and Figure 6b). In the Δ*rnf* mutant, a "headless" Fpo complex might serve as a new entry point for electrons from ferredoxin (Figure 5b; Supplementary Figure 2) in the ETC (32), whereas acetyl CoA synthesis mediated by CODH/ACS could possibly regenerate the reduced ferredoxin pool the Δ*mmcA* mutant (Figure 6b) (26). The "headless" Fpo backup strategy is coupled to proton translocation

and would theoretically conserve more energy for the Δ*rnf* mutant compared to the CODH/ACS strategy in the Δ*mmcA* mutant. Accordingly, the Δ*rnf* mutant has faster growth rate than then Δ*mmcA* mutants on methylated compounds (Figure 3). We anticipate that the potential alternative strategies for ferredoxin regeneration stem from distinct regulatory responses by the cell to the loss of either MmcA or the entire Rnf complex. Our transcriptomic data corroborates this hypothesis, in which we saw upregulation of the global methanogenesis protein MreA in the Δ*mmcA* mutant but not the Δ*rnf* mutant (Figure 6; Supplementary Table 9). Higher expression of MreA would lower the expression of *fpo* locus in the Δ*mmcA* mutant during methylotrophic methanogenesis (52). Similarly, induction of MreA during acetoclastic growth might also explain the lethal phenotype for both mutants (52). These data showcase the sheer diversity of energy conservation strategies present in *M. acetivorans*, and likely other members of the *Methanosarcinales*, which enable these organisms to thrive in a wide array of ecological niches.

Additionally, based on our phenotypic (Figure 3 and Figure 4) and transcriptomic analyses (Figures 5 and Figure 6), we observe that the impact of deleting the Rnf complex or MmcA extends far beyond energy conservation in the cell. Genes involved in Na^+ ion transport, amino acid biosynthetic pathways, substrate specific methyltransferases for methylotrophic methanogenesis, transcriptional regulators, and many other loci were differentially expressed in one or both mutants (Figure 5 and Figure 6). These dramatic transcriptional changes underscore a complex and intricate regulatory network that connects carbon transformation by methyltransferases and energy conservation during methanogenic growth. Further analyses of regulatory genes identified in this work and similar studies with other components of the ETC will ultimately provide systems-level insights into methanogenesis in *Methanosarcina acetivorans,* and will deepen our understanding of these ecologically-relevant microbes.

Materials and Methods

Media and culture conditions. All *Methanosarcina* strains were grown at 37ºC without shaking in bicarbonate-buffered high-salt (HS) liquid medium containing either 50 mM trimethylamine hydrochloride (TMA), 125 mM methanol, 40 mM sodium acetate, or 20 mM dimethylsulfide (DMS) as a growth substrate (56). TMA, methanol, and acetate were added prior to autoclaving whereas DMS was added after autoclaving from a 200 mM stock solution prepared in HS medium with no other carbon sources. For mutant generation, the growth medium contained 50 mM TMA as the growth substrate and agar solidified HS + TMA media was obtained by adding 1.5% w/v agar (Sigma-Aldrich, St. Louis, MO, USA). To select for transformants, puromycin (Pur) (RPI, Mount Prospect, IL, USA) was added to HS + TMA agar medium before solidification to a final concentration of 2 ug/mL from a 1000X sterile, anaerobic stock solution with N_2 gas in the headspace at 55-69 kPa. HS + TMA + Pur agar plates were incubated at 37ºC in an intra-chamber anaerobic incubator with $N_2/CO_2/H_2S$ (79.9%/20%/0.1%) in the headspace, as described previously (57). All *Escherichia coli* strains were grown in Lysogeny broth (LB) at 37ºC in a shaking incubator (Thermo Fisher Scientific, Waltham, MA, USA) at 250 rpm. To select for the desired plasmids, antibiotics were added to cultures to final concentrations of 25 µg/mL for kanamycin, and/or 10 µg/mL for chloramphenicol as listed in Supplementary Table 10. For plasmid extraction, rhamnose was added to a final concentration of 10 mM to *E. coli* cultures prior to incubation to increase the plasmid copy number of pDN201- and pJK029A-derived plasmids.

Construction of *Methanosarcina acetivorans* mutants. Liposome-mediated transformation of *M. acetivorans* was performed as previously described (58). Briefly, 20 mL of late-exponential phase (~0.8 OD_{600}) cultures growing on HS + TMA were harvested by centrifugation, the

supernatant was decanted, and the cell pellet was resuspended in 1 mL of anaerobic bicarbonate-buffered, isotonic sucrose (pH = 7.4) containing 100 µM cysteine. Next, 25 uL of N-[1-(2,3-Dioleoyloxy)propyl]-N,N,N-trimethylammonium methylsulfate (DOTAP) (Roche Diagnostics Deutschland GmbH, Mannheim, Germany) and 2 ug of plasmid DNA were incubated for 30 mins in 75 uL of buffered, isotonic sucrose to allow for DNA uptake into liposomes. After incubation, the DOTAP + DNA mixture was added in full to the cell suspensions. Suspensions of cells + DOTAP + DNA were incubated for 4 hours at room temperature in an anaerobic chamber with $CO_2/H_2/N_2$ (10/5/85) in the headspace before inoculation into 10 mL of HS + TMA. Outgrowths of transformed cells were incubated at 37ºC for 12-16 hours before plating on agar-solidified HS + Pur + TMA using a sterile spreader (56). Plasmids used for mutant generation are described in Supplementary Table 10. Mutant colonies were genotyped using primers detailed in Supplementary Table 11, and a full list of strains used in this study is provided in Supplementary Table 12.

Growth Assays for *Methanosarcina acetivorans* mutants. For growth analysis, 11 mL cultures were grown at 37ºC without shaking (HeraTherm™General Protocol Microbiological Incubator, Thermo Fisher Scientific, Waltham, MA, USA) in Balch tubes with N_2/CO_2 (80/20) at 55-69 kPa in the headspace. Growth of three independent biological replicates was measured by determining the optical density of cultures at 600nm (OD_{600}) using a UV-Vis Spectrophotometer (Gensys 50, Thermo Fisher Scientific, Waltham, MA, USA). A Balch tube containing 10 mL of HS medium with the appropriate growth substrate was used as a 'blank' for optical density measurements. For growth on TMA or methanol, cells were acclimated to the growth substrate for a minimum of four generations prior to quantitative growth measurements. Growth measurements on acetate and DMS were performed with cells previously grown on TMA.

Approximately 1 mL of late exponential phase culture was harvested and served as the inoculum into 10 mL of fresh medium for growth analyses. Growth data were log10-transformed and plotted versus time. A linear regression was fitted to the data to include at least 5 data points on the growth curve for a regression coefficient (R^2) ≥ 0.97. Growth rate (gr) was calculated as the slope of the linear fit multiplied by 2.303, and the doubling time was calculated as T_d = 0.6932/gr. Lag time was calculated by subtracting the Y-intercept value from the log10-transformed initial OD_{600} reading and dividing by the slope of the linear fit. For maximum OD_{600} measurements, approximately 1 mL of early stationary phase culture was harvested and diluted into 10 mL of fresh HS medium containing the same substrate used for growth. An OD_{600} measurement of the diluted culture was then multiplied by 11 to approximate the maximum OD_{600} value. Growth curve plots, determination of doubling time, lag time, and statistical analyses were obtained using Microsoft Excel Version 16.55. Plots of OD_{600} versus time were generated using GraphPad/Prism 9.3.1.

DNA extraction and sequencing. Cells from a 10 ml culture of DDN009 (Δ*mmcA*) incubated in in HS + TMA at 37 ^{o}C were harvested at late-exponential phase (OD_{600} ~0.8) for genomic DNA extraction using the Qiagen blood and tissue kit (Qiagen, Hilden, Germany). The concentration of genomic DNA was measured using a Nanodrop One Microvolume UV-Vis Spectrophotmeter (Thermo Scientific, Waltham, MA, USA). Genomic DNA was shipped to the Microbial Genome Sequencing Center, Pittsburgh, PA, USA, where sequencing libraries preparation and sequencing was performed. Sequencing reads were aligned to the *Methanosarcina acetivorans* C2A genome and mutations were identified using Breseq version 0.35.5. Illumina sequencing reads for DDN009 have been deposited to the Sequencing Reads Archive (SRA) and the BioProject accession number will be made available upon publication.

RNA extraction and sequencing. WWM60 (parent), WWM1015 (Δ*rnf*) and DDN009 (Δ*mmcA*) pre-acclimated on TMA were inoculated in quadruplicate from late exponential phase cultures (OD_{600} ~0.8) into 10mL of fresh HS + TMA in Balch tubes with N_2/CO_2 (80/20) at 55-69 kPa in the headspace and grown at 37ºC without shaking (Isotemp™ Microbiological Incubator, Thermo Fisher Scientific, Waltham, MA, USA). One Balch tube was used to monitor growth as a proxy for the other replicates by measuring the OD_{600} routinely using a UV-Vis Spectrophotometer (Gensys 50, Thermo Fisher Scientific, Waltham, MA, USA). Once the measured OD_{600} reached approximately ½ maximum value (0.750-0.850), RNA was harvested from the remaining three culture tubes. For RNA extraction, 1 mL of culture was added to 1 mL of Trizol pre-warmed to 37ºC (Life Technologies, Carlsbad, CA, USA) and incubated at room temperature for 5 minutes. Next, 2 mL of 100% ethanol was added to each sample and RNA extraction was performed using the Qiagen RNeasy Mini Kit (Qiagen, Hilden, Germany) according to the manufacturer's instructions. The concentration and quality of RNA samples was determined using a Nanodrop One/One^C UV Spectrophotometer (Thermo Fisher Scientific, Waltham, MA, USA) before storage at -80ºC. Samples were submitted to the Microbial Genome Sequencing Center (Pittsburg, PA) for DNase treatment, rRNA depletion, library preparation, and Illumina paired-end sequencing. On average 98% of reads were mapped to the *M. acetivorans* C2A genome. Raw transcript reads were deposited to the Sequence Read Archive (SRA) and the BioProject accession number will be made available upon publication.

RNAseq analysis. Reads in FASTQ format were uploaded to KBase in a new 'Narrative': a Jupyter-based user interface in which the raw reads are processed using 'apps' and the output/result of each app is recorded and accessible for download (59). Raw transcript reads were grouped by strain in a 'SampleSet' using the app 'Create RNA-seq SampleSet'. Next, the

SampleSet was selected as input for read alignment using the HISAT2 (v.2.1.0) app with the *Methanosarcina acetivorans* C2A genome serving as the reference for mapping. Aligned reads were assembled using the Cufflinks (v2.2.1) app with the *M. acetivorans* C2A genome input as the reference. The output of Cufflinks was exported an Expression Set and individual expression matrices for each strain and associated replicates. The expression values for each gene were reported as $\log_2$(FPKM) (fragments per kilobase per million mapped reads). Finally, differential expression matrices for each pairwise combination of strains were generated by uploading the $\log_2$(FPKM) Expression Set to the DESeq2 (v1.20.0) app. Changes in transcript abundance were considered significant between strains if a $\geq \pm 2$ $\log_2$-fold (q-values ≤ 0.05) change was seen. Differential expression of genes was visualized in volcano plots constructed using a Python script and a table with the locus tag, $\log_2$-fold change in expression, q-value, and assigned color for each gene. Before plotting, select genes were highlighted in colors other than gray by manual curation of the table in Microsoft Excel (version 16.62), and genes with a q-value of zero were assigned a value of 1E-300. Volcano plots show $\log_2$-fold change on the x-axis and $\log_{10}$(q-value) on the y-axis for each gene.

Funding Information

The authors acknowledge funding from the Beckman Young Investigator Award sponsored by the Arnold and Mabel Beckman Foundation (to D.D.N and B.E.D), 'New Tools for Advancing Model Systems in Aquatic Symbiosis' program from the Gordon and Betty Moore Foundation (GBMF#9324) (to D.D.N and D.G), the Simons Early Career Investigator in Marine Microbial Ecology and Evolution Award (to D.D.N), the Searle Scholars Program sponsored by the Kinship Foundation (to D.D.N), the Rose Hills Innovator Grant (to D.D.N), the Packard Fellowship in Science and Engineering sponsored by the David and Lucille Packard Foundation

(to D.D.N), funding from the Shurl and Kay Curci Foundation (to D.D.N), the NIH 'Genetic Dissection of Cells and Organisms' training program (award #5T32GM132022-03) (to B.E.D.), and startup funds from the Department of Molecular and Cell Biology at UC Berkeley (to D.D.N). D.D.N is a Chan Zuckerberg Biohub Investigator. The funders had no role in the conceptualization and writing of this manuscript or the decision to submit the work for publication.

Acknowledgements

The authors would like to acknowledge Katie Shalvarjian for assistance with data visualization and other members of the Nayak lab for their feedback and input.

Competing Interests

The authors do not declare any competing interests.

Figure Legends

Figure 1. a) Schematic of the electron transport chain in *Methanosarcina acetivorans* depicting energy conservation facilitated by two respiratory complexes: 1) the F_{420} dehydrogenase complex in (Fpo) in blue and the *Rhodobacter* nitrogen fixation complex (Rnf) in red along with the terminal electron accepting complex HdrDE in green. **b)** Model of the six-subunit Rnf complex from the bacterium, *Acetobacterium woodii*, which serves as a reversible Na^+-pumping Ferredoxin (Fd):NAD^+ oxidoreductase (20). Note: the Rnf complex found in members of the *Methanosarcinales* couples the transfer of electrons between the cytosolic Fd pool and the membrane-bound MP pool to sodium translocation. The exact pathway of electron flow from Fd to MP is unknown. Additionally, in the *Methanosarcinales*, Rnf contains eight subunits instead of six, one of which is a multiheme c-type cytochrome, MmcA.

Figure 2. a) Chromosomal organization of the eight-gene *rnf* operon in *M. acetivorans*, reflecting the genotype of the parent strain (WWM60) used in this study. Locus tags are provided under each gene. **b)** Chromosomal organization the *rnf* locus in the Δ*rnf* mutant showing a clean deletion of the operon. A 30 basepair (bp) region of the 5' end of *mmcA* and a 30 bp region of at the 3' end of *rnfX* are maintained on the chromosome to preclude interference with up- and down-stream regulatory elements outside of the operon. **c)** Chromosomal organization of the *rnf* locus in the Δ*mmcA* mutant. Here, 30 bp regions at the 5' and 3' ends of *mmcA* are maintained to prevent frameshift disruption of downstream *rnf* genes. **d)** Expression values for the *rnf* genes in the parent and Δ*mmcA* strains. Expression is measured in $\log_2$(FPKM) [fragments per kilobase of transcript per million mapped reads] for each gene. In the Δ*mmcA* strain, only *mmcA* expression is abolished [p-value = 3.5E-9; Welch's t-test] indicating the deletion does not adversely impact

617 on the expression of other genes in the operon. Significance (p-values < 0.05) for $\log_2$(FPKM)
618 values of individual genes between strains is indicated with an asterisk or "ns" for non-
619 significant change. **e)** Growth curve of the parent strain carrying an empty vector control (light
620 gray circles), the Δ*mmcA* mutant carrying an empty vector control (dark gray diamonds), and the
621 Δ*mmcA* mutant carrying a plasmid expressing *mmcA* (pink inverted triangles) in HS medium
622 containing 50 mM TMA as the sole carbon and energy source. The empty vector contains the β-
623 glucuronidase gene, *uidA*, under the control of a tetracycline inducible P*mcrB* (*tetO4*) promoter
624 described previously in (60). The complementation vector contains *mmcA* under the control of a
625 tetracycline inducible P*mcrB* (*tetO4*) promoter described previously in (24). Three replicate
626 tubes of each strain were used for growth assays and tetracycline was added to a final
627 concentration of 100 ug/mL in the growth medium.
628
629 **Figure 3.** Growth curves of the parent strain (WWM60) (blue circles), Δ*rnf* (green diamonds),
630 and Δ*mmcA* (orange inverted triangles) mutants on **a)** 40 mM acetate, **b)** 50 mM trimethylamine
631 (TMA), **c)** 125 mM MeOH, and **d)** 20 mM dimethylsulfide (DMS) as the sole carbon and energy
632 source. Three replicate tubes of each strain were used for growth assays.
633
634 **Figure 4. a)** Growth curve of the parent strain (WWM60) (blue circles), Δ*rnf* (green diamonds),
635 and Δ*mmcA* (orange inverted triangles) mutants in HS medium containing 20 mM
636 dimethylsulfide (DMS) as the sole carbon and energy source after transfer from HS medium with
637 50 mM trimethylamine (TMA) as the sole carbon and energy source. **b)** A schematic depicting
638 the genotype of a strain generated to assay the role of *mmcA* in the absence of the rest of the *rnf*
639 genes. On the chromosome, the entire *rnf* locus has been deleted. The strain carries an

640 autonomously replicating plasmid encoding *mmcA* with a tandem-affinity-purification (TAP) tag
641 at the C-terminus under the control of a P*mcrB* promoter described previously in (60). **c)** Growth
642 curve of the Δ*rnf* strain carrying an empty vector control (dark gray circles) or a plasmid
643 expressing *mmcA* (light blue diamonds) in HS medium containing 50 mM TMA as the sole
644 carbon and energy source. The empty vector contains the β-glucuronidase gene, *uidA*, under the
645 control of a P*mcrB* promoter described previously in (60). Three replicate tubes of each strain
646 were used for growth assays.
647
648 **Figure 5. a)** Volcano plot showing the differential expression of genes between the Δ*mmcA* and
649 Δ*rnf* mutants. Genes with higher expression in the Δ*mmcA* mutant have a positive $\log_2$-fold
650 change value, while genes with higher expression in the Δ*rnf* mutant have a negative $\log_2$-fold
651 change value. Dashed lines on the plot delineate the cutoff for 'significant' $\log_2$-fold change in
652 transcript abundance in either mutant. In the Δ*rnf* mutant, two sets of genes are significantly
653 more highly expressed: six subunits of the Fpo complex (shaded in blue), and multiple
654 methylamine methyltransferases and permeases (shaded in green). Genes in orange have higher
655 transcript levels in the Δ*mmcA* mutant relative to both the Δ*rnf* mutant and the parent strain
656 (WWM60), genes in gold have significantly lower transcript levels in the Δ*rnf* mutant relative to
657 both the Δ*mmcA* mutant and WWM60, whereas genes in red are uniquely upregulated in the
658 Δ*mmcA* mutant compared to the Δ*rnf* mutant. The seven remaining genes of the Rnf complex in
659 the Δ*mmcA* mutant are shaded in maroon. **b)** Chromosomal organization of the thirteen-gene *fpo*
660 operon in *M. acetivorans*, and the additional *fpoO2* and *fpoF* genes. Double vertical lines
661 indicate genes are located more than 3 kbp away in the genome. The $\log_2$-fold change in
662 transcript abundance for each gene in the Fpo complex for all pairwise comparisons between the

663 Δ*mmcA* mutant, the Δ*rnf* mutant, and WWM60 are shown in the bar graph. The dashed line on
664 the plot delineates the cutoff for 'significant' $\log_2$-fold change in transcript abundance. In the bar
665 graph: light blue bars represent the expression in the Δ*mmcA* mutant compared to the Δ*rnf*
666 mutant, with higher expression in the Δ*mmcA* mutant denoted by a positive $\log_2$-fold change.
667 Medium blue bars represent the expression in the Δ*rnf* mutant compared to the parent strain, with
668 higher expression in the Δ*rnf* mutant denoted by a positive $\log_2$-fold change. Dark blue bars
669 represent the expression in the Δ*mmcA* mutant compared to the parent strain, with higher
670 expression in the Δ*mmcA* strain denoted by a positive $\log_2$-fold change. **c)** Chromosomal
671 organization of four different methylamine methyltransferase loci. The $\log_2$-fold change in
672 transcript abundance for each gene at the various loci for all pairwise comparisons between the
673 Δ*mmcA* mutant, the Δ*rnf* mutant, and WWM60 are shown in the bar graphs. The dashed lines on
674 the plots delineate the cutoff for 'significant' $\log_2$-fold change in transcript abundance. In both
675 bar graphs: light green bars represent the expression in the Δ*mmcA* mutant compared to the Δ*rnf*
676 mutant, with higher expression in the Δ*mmcA* mutant denoted by a positive $\log_2$-fold change.
677 Medium green bars represent the expression in the Δ*rnf* mutant compared to the parent strain,
678 with higher expression in the Δ*rnf* mutant denoted by a positive $\log_2$-fold change. Dark green
679 bars represent the expression in the Δ*mmcA* mutant compared to the parent strain, with higher
680 expression in the Δ*mmcA* strain denoted by a positive $\log_2$-fold change.
681
682 **Figure 6. a)** Volcano plot showing the differential expression of genes between the Δ*rnf* and the
683 parent strain (WWM60). Genes with higher expression in the Δ*rnf* mutant have a positive $\log_2$-
684 fold change value, while genes with higher expression in the parent have a negative $\log_2$-fold
685 change value. Dashed lines on the plot delineate the cutoff for 'significant' $\log_2$-fold change in

686 transcript abundance in either strain. Genes in light purple are significantly differentially
687 expressed in both the Δ*rnf* and Δ*mmcA* mutant relative to the WWM60. Genes in dark magenta
688 have significant differential expression only in the Δ*rnf* mutant relative to WWM60. **b)** Volcano
689 plot
690 showing the differential expression of genes between the Δ*mmcA* and the parent strain
691 (WWM60). Genes with higher expression in the Δ*mmcA* mutant have a positive log_2-fold change
692 value, while genes with higher expression in the parent have a negative log_2-fold change value.
693 Dashed lines on the plot delineate the cutoff for 'significant' log_2-fold change in transcript
694 abundance in either strain. Genes in light purple are significantly differentially expressed in both
695 the Δ*rnf* and Δ*mmcA* mutant relative to the parent strain. Genes in dark purple have significant
696 differential expression only in the Δ*mmcA* mutant relative to the parent. **c)** Schematic of the Na^+-
697 translocating F1F0 ATP synthase in *M. acetivorans*. ATP hydrolysis results in the translocation
698 of three sodium ions across the cell membrane to maintain the sodium gradient in the absence of
699 a fully functional Rnf complex (44). Subunits with significant fold change are shaded in orange.
700 The log_2-fold change in transcript abundance for every gene in the F1F0 ATP synthase between
701 the Δ*rnf* mutant (black bars) and the Δ*mmcA* mutant (gray bars) compared to WWM60 are
702 shown in the bar graph. The dashed line on the plot delineates the cutoff for a 'significant' log_2-
703 fold change in transcript abundance. **d)** Chromosomal organization of the *cdh1* operon in *M.*
704 *acetivorans*. The log_2-fold change in transcript abundance for each gene in the *cdh1* operon
705 between the Δ*rnf* mutant (black bars) and the Δ*mmcA* mutant (gray bars) compared to WWM60
706 are shown in the bar graph. The dashed line on the plot delineates the cutoff for a 'significant'
707 log_2-fold change in transcript abundance.
708

References

1. Dean JF, Middelburg JJ, Röckmann T, Aerts R, Blauw LG, Egger M, Jetten MSM, de Jong AEE, Meisel OH, Rasigraf O, Slomp CP, in't Zandt MH, Dolman AJ. 2018. Methane feedbacks to the global climate system in a warmer world. Rev Geophys 56:207–250.

2. Thauer RK, Kaster A-K, Seedorf H, Buckel W, Hedderich R. 2008. Methanogenic archaea: ecologically relevant differences in energy conservation. Nat Rev Microbiol 6:579–591.

3. Thauer RK 1998. Biochemistry of methanogenesis: a tribute to Marjory Stephenson: 1998 Marjory Stephenson Prize Lecture. Microbiology 144:2377–2406.

4. Mand TD, Metcalf WW. 2019. Energy conservation and hydrogenase function in methanogenic archaea, in particular the genus *Methanosarcina*. Microbiol Mol Biol Rev 83:e00020-19.

5. Abken H-J, Tietze M, Brodersen J, Bäumer S, Beifuss U, Deppenmeier U. 1998. Isolation and characterization of methanophenazine and function of phenazines in membrane-bound electron transport of *Methanosarcina mazei* Gö1. J Bacteriol 180:2027–2032.

6. DiMarco AA, Bobik TA, Wolfe RS. Unusual coenzymes of methanogenesis. 1990. Annu Rev Biochem 59:355-394.

7. Künkel A, Vaupel M, Heim S, Thauer RK, Hedderich R. 1997. Heterodisulfide reductase from methanol-grown cells of *Methanosarcina barkeri* is not a flavoenzyme. Eur J Biochem 244:226–234.

728 8. Buan NR, Metcalf WW. 2010. Methanogenesis by *Methanosarcina acetivorans* involves two
729 structurally and functionally distinct classes of heterodisulfide reductase. Mol Microbiol
730 75:843–853.

731 9. Simianu M, Murakami E, Brewer JM, Ragsdale SW. 1998. Purification and properties of the
732 heme- and iron−sulfur-containing heterodisulfide reductase from *Methanosarcina*
733 *thermophila*. Biochemistry 37:10027–10039.

734 10. Kulkarni G, Kridelbaugh DM, Guss AM, Metcalf WW. 2009. Hydrogen is a preferred
735 intermediate in the energy-conserving electron transport chain of *Methanosarcina barkeri*.
736 Proc Natl Acad Sci USA 106:15915–15920.

737 11. Kulkarni G, Mand TD, Metcalf WW. 2018. Energy conservation via hydrogen cycling in the
738 methanogenic archaeon *Methanosarcina barkeri*. mBio 9:e01256-18.

739 12. Mand TD, Kulkarni G, Metcalf WW. 2018. Genetic, biochemical, and molecular
740 characterization of *Methanosarcina barkeri* mutants lacking three distinct classes of
741 hydrogenase. J Bacteriol 200:e00342-18.

742 13. Guss AM, Kulkarni G, Metcalf WW. 2009. Differences in hydrogenase gene expression
743 between *Methanosarcina acetivorans* and *Methanosarcina barkeri*. J Bacteriol 191:2826–
744 2833.

745 14. Galagan JE, Nusbaum C, Roy A, Endrizzi MG, Macdonald P, FitzHugh W, Calvo S, Engels
746 R, Smirnov S, Atnoor D, Brown A, Allen N, Naylor J, Stange-Thomann N, DeArellano K,
747 Johnson R, Linton L, McEwan P, McKernan K, Talamas J, Tirrell A, Ye W, Zimmer A,
748 Barber RD, Cann I, Graham DE, Grahame DA, Guss AM, Hedderich R, Ingram-Smith C,

749 Kuettner HC, Krzycki JA, Leigh JA, Li W, Liu J, Mukhopadhyay B, Reeve JN, Smith K,
750 Springer TA, Umayam LA, White O, White RH, Macario EC de, Ferry JG, Jarrell KF, Jing
751 H, Macario AJL, Paulsen I, Pritchett M, Sowers KR, Swanson RV, Zinder SH, Lander E,
752 Metcalf WW, Birren B. 2002. The genome of *M. acetivorans* reveals extensive metabolic
753 and physiological diversity. Genome Res 12:532–542.

754 15. Schlegel K, Welte C, Deppenmeier U, Müller V. 2012. Electron transport during aceticlastic
755 methanogenesis by *Methanosarcina acetivorans* involves a sodium-translocating Rnf
756 complex. FEBS J 279:4444–4452.

757 16. Bäumer S, Ide T, Jacobi C, Johann A, Gottschalk G, Deppenmeier U. 2000. The F420H2
758 dehydrogenase from *Methanosarcina mazei* is a redox-driven proton pump closely related to
759 NADH dehydrogenases. J Biol Chem 275:17968–17973.

760 17. Friedrich T, Steinmüller K, Weiss H. 1995. The proton-pumping respiratory complex I of
761 bacteria and mitochondria and its homologue in chloroplasts. FEBS Lett 367:107–111.

762 18. Li Q, Li L, Rejtar T, Lessner DJ, Karger BL, Ferry JG. 2006. Electron transport in the
763 pathway of acetate conversion to methane in the marine archaeon *Methanosarcina*
764 *acetivorans*. J Bacteriol 188:702–710.

765 19. Wang M, Tomb J-F, Ferry JG. 2011. Electron transport in acetate-grown *Methanosarcina*
766 *acetivorans*. BMC Microbiol 11:165.

767 20. Biegel E, Schmidt S, González JM, Müller V. 2011. Biochemistry, evolution and
768 physiological function of the Rnf complex, a novel ion-motive electron transport complex in
769 prokaryotes. Cell Mol Life Sci 68:613–634.

770 21. Hreha TN, Mezic KG, Herce HD, Duffy EB, Bourges A, Pryshchep S, Juarez O, Barquera B.
771 2015. Complete topology of the RNF Complex from *Vibrio cholerae*. Biochemistry
772 54:2443–2455.

773 22. Holmes DE, Ueki T, Tang H-Y, Zhou J, Smith JA, Chaput G, Lovley DR. 2019. A
774 membrane-bound cytochrome enables *Methanosarcina acetivorans* to conserve energy from
775 extracellular electron transfer. mBio 10:e00789-19.

776 23. Mand TD. 2018. Hydrogenase utilization and regulation in species of *Methanosarcina*.
777 University of Illinois at Urbana-Champaign, Urbana-Champaign, IL.

778 24. Gupta D, Shalvarjian KE, Nayak DD. 2022. An archaea-specific *c*-type cytochrome
779 maturation machinery is crucial for methanogenesis in *Methanosarcina acetivorans*. eLife
780 11:e76970.

781 25. Nayak DD, Metcalf WW. 2017. Cas9-mediated genome editing in the methanogenic
782 archaeon *Methanosarcina acetivorans*. Proc Natl Acad Sci USA 114:2976–2981.

783 26. Terlesky KC, Ferry JG. 1988. Ferredoxin requirement for electron transport from the carbon
784 monoxide dehydrogenase complex to a membrane-bound hydrogenase in acetate-grown
785 *Methanosarcina thermophila*. J Biol Chem 263:4075–4079.

786 27. Li Q, Li L, Rejtar T, Karger BL, Ferry JG. 2005. Proteome of *Methanosarcina acetivorans*
787 Part II: comparison of protein levels in acetate- and methanol-grown cells. J Proteome Res
788 4:129–135.

789 28. Hippe H, Caspari D, Fiebig K, Gottschalk G. 1979. Utilization of trimethylamine and other
790 N-methyl compounds for growth and methane formation by *Methanosarcina barkeri*. Proc
791 Natl Acad Sci USA 76:494–498.

792 29. Pritchett MA, Metcalf WW. 2005. Genetic, physiological and biochemical characterization
793 of multiple methanol methyltransferase isozymes in *Methanosarcina acetivorans* C2A. Mol
794 Microbiol 56:1183–1194.

795 30. Oelgeschläger E, Rother M. 2009. *In vivo* role of three fused corrinoid/methyl transfer
796 proteins in *Methanosarcina acetivorans*. Mol Microbiol 72:1260–1272.

797 31. Deppenmeier U. 2004. The membrane-bound electron transport system of *Methanosarcina*
798 species. J Bioenerg Biomembr 36:55–64.

799 32. Welte C, Deppenmeier U. 2011. Membrane-bound electron transport in *Methanosaeta*
800 *thermophila*. J Bacteriol 193:2868–2870.

801 33. Burke SA, Lo SL, Krzycki JA. 1998. Clustered genes encoding the methyltransferases of
802 methanogenesis from monomethylamine. J Bacteriol 180:3432–3440.

803 34. Paul L, Ferguson DJ, Krzycki JA. 2000. The trimethylamine methyltransferase gene and
804 multiple dimethylamine methyltransferase genes of *Methanosarcina barkeri* contain in-
805 frame and read-through amber codons. J Bacteriol 182:2520–2529.

806 35. Scofield MA, Lewis WS, Schuster SM. 1990. Nucleotide sequence of *Escherichia coli asnB*
807 and deduced amino acid sequence of asparagine synthetase B. J Biol Chem 265:12895–
808 12902.

809 36. Jarrell KF, Jones GM, Nair DB. 2010. Biosynthesis and role of N-Linked glycosylation in
810 cell surface structures of archaea with a focus on flagella and S layers. Int J Microbiol
811 2010:e470138.

812 37. Vander Horn PB, Backstrom AD, Stewart V, Begley TP. 1993. Structural genes for thiamine
813 biosynthetic enzymes (*thiCEFGH*) in *Escherichia coli* K-12. J Bacteriol 175:982–992.

814 38. Holmes DE, Rotaru A-E, Ueki T, Shrestha PM, Ferry JG, Lovley DR. 2018. Electron and
815 proton flux for carbon dioxide reduction in *Methanosarcina barkeri* during direct
816 interspecies electron transfer. Front Microbiol 9:3109.

817 39. De Pina K, Desjardin V, Mandrand-Berthelot M-A, Giordano G, Wu L-F. 1999. Isolation
818 and characterization of the *nikR* gene encoding a nickel-responsive regulator in *Escherichia*
819 *coli*. J Bacteriol 181:670–674.

820 40. Zhou Y, Wang L, Yang F, Lin X, Zhang S, Zhao ZK. 2011. Determining the extremes of the
821 cellular NAD(H) Level by using an *Escherichia coli* NAD+-auxotrophic mutant. Appl
822 Environ Microbiol 77:6133–6140.

823 41. Paula FS, Chin JP, Schnürer A, Müller B, Manesiotis P, Waters N, Macintosh KA, Quinn JP,
824 Connolly J, Abram F, McGrath JW, O'Flaherty V. 2019. The potential for polyphosphate
825 metabolism in archaea and anaerobic polyphosphate formation in *Methanosarcina mazei*. Sci
826 Rep 9:17101.

827 42. Rosenberg H, Gerdes RG, Chegwidden K. 1977. Two systems for the uptake of phosphate in
828 *Escherichia coli*. J Bacteriol 131(2):505-511

829 43. Schlegel K, Leone V, Faraldo-Gómez JD, Müller V. 2012. Promiscuous archaeal ATP
830 synthase concurrently coupled to Na^+ and H^+ translocation. Proc Natl Acad Sci USA
831 109:947–952.

832 44. Saum R, Schlegel K, Meyer B, MÃ¼ller V. 2009. The F_1 F_O ATP synthase genes in
833 *Methanosarcina acetivorans* are dispensable for growth and ATP synthesis. FEMS
834 Microbiol Lett 300:230–236.

835 45. Walker JE. 2013. The ATP synthase: the understood, the uncertain and the unknown.
836 Biochem Soc Trans 41:1–16.

837 46. Jasso-Chavez R, Apolinario EE, Sowers KR, Ferry JG. 2013. MrpA functions in energy
838 conversion during acetate-dependent growth of *Methanosarcina acetivorans*. J Bacteriol
839 195:3987–3994.

840 47. Fu H, Metcalf WW. 2015. Genetic basis for metabolism of methylated sulfur compounds in
841 *Methanosarcina* species. J Bacteriol 197:1515–1524.

842 48. Lacasse MJ, Zamble DB. 2016. [NiFe]-hydrogenase maturation. Biochemistry 55:1689–
843 1701.

844 49. Brey RN, Rosen BP, Sorensen EN. 1980. Cation/proton antiport systems in *Escherichia coli*.
845 Properties of the potassium/proton antiporter. J Biol Chem 255:39–44.

846 50. Matschiavelli N, Oelgeschläger E, Cocchiararo B, Finke J, Rother M. 2012. Function and
847 regulation of isoforms of carbon monoxide dehydrogenase/acetyl coenzyme A synthase in
848 *Methanosarcina acetivorans*. J Bacteriol 194:5377–5387.

849 51. Hovey R, Lentes S, Ehrenreich A, Salmon K, Saba K, Gottschalk G, Gunsalus RP,
850 Deppenmeier U. 2005. DNA microarray analysis of *Methanosarcina mazei* Gö1 reveals
851 adaptation to different methanogenic substrates. Mol Genet Genomics 273:225–239.

852 52. Reichlen MJ, Vepachedu VR, Murakami KS, Ferry JG. 2012. MreA functions in the global
853 regulation of methanogenic pathways in *Methanosarcina acetivorans*. mBio 3:e00189-12.

854 53. Gaston MA, Jiang R, Krzycki JA. 2011. Functional context, biosynthesis, and genetic
855 encoding of pyrrolysine. Curr Opin Microbiol 14:342–349.

856 54. Zheng K, Ngo PD, Owens VL, Yang X, Mansoorabadi SO. 2016. The biosynthetic pathway
857 of coenzyme F430 in methanogenic and methanotrophic archaea. Science 354:339–342.

858 55. Moore SJ, Sowa ST, Schuchardt C, Deery E, Lawrence AD, Ramos JV, Billig S, Birkemeyer
859 C, Chivers PT, Howard MJ, Rigby SEJ, Layer G, Warren MJ. 2017. Elucidation of the
860 biosynthesis of the methane catalyst coenzyme F430. Nature 543:78–82.

861 56. Sowers KR, Boone JE, Gunsalus RP. 1993. Disaggregation of *Methanosarcina* spp. and
862 growth as single cells at elevated osmolarity. Appl Environ Microbiol 59:3832–3839.

863 57. Metcalf WW, Zhang JK, Wolfe RS. 1998. An anaerobic, intrachamber incubator for growth
864 of *Methanosarcina* spp. on methanol-containing solid media. Appl Environ Microbiol
865 64:768–770.

866 58. Metcalf WW, Zhang JK, Apolinario E, Sowers KR, Wolfe RS. 1997. A genetic system for
867 archaea of the genus *Methanosarcina*: liposome-mediated transformation and construction of
868 shuttle vectors. Proc Natl Acad Sci USA 94:2626–2631.

869 59. Arkin AP, Cottingham RW, Henry CS, Harris NL, Stevens RL, Maslov S, Dehal P, Ware D,
870 Perez F, Canon S, Sneddon MW, Henderson ML, Riehl WJ, Murphy-Olson D, Chan SY,
871 Kamimura RT, Kumari S, Drake MM, Brettin TS, Glass EM, Chivian D, Gunter D, Weston
872 DJ, Allen BH, Baumohl J, Best AA, Bowen B, Brenner SE, Bun CC, Chandonia J-M, Chia
873 J-M, Colasanti R, Conrad N, Davis JJ, Davison BH, DeJongh M, Devoid S, Dietrich E,
874 Dubchak I, Edirisinghe JN, Fang G, Faria JP, Frybarger PM, Gerlach W, Gerstein M,
875 Greiner A, Gurtowski J, Haun HL, He F, Jain R, Joachimiak MP, Keegan KP, Kondo S,
876 Kumar V, Land ML, Meyer F, Mills M, Novichkov PS, Oh T, Olsen GJ, Olson R, Parrello
877 B, Pasternak S, Pearson E, Poon SS, Price GA, Ramakrishnan S, Ranjan P, Ronald PC,
878 Schatz MC, Seaver SMD, Shukla M, Sutormin RA, Syed MH, Thomason J, Tintle NL,
879 Wang D, Xia F, Yoo H, Yoo S, Yu D. 2018. KBase: The United States Department of
880 Energy systems biology knowledgebase. Nat Biotechnol 36:566–569.

881 60. Guss AM, Rother M, Zhang JK, Kulkkarni G, Metcalf WW. 2008. New methods for tightly
882 regulated gene expression and highly efficient chromosomal integration of cloned genes for
883 *Methanosarcina* species. Archaea 2:193–203.

884

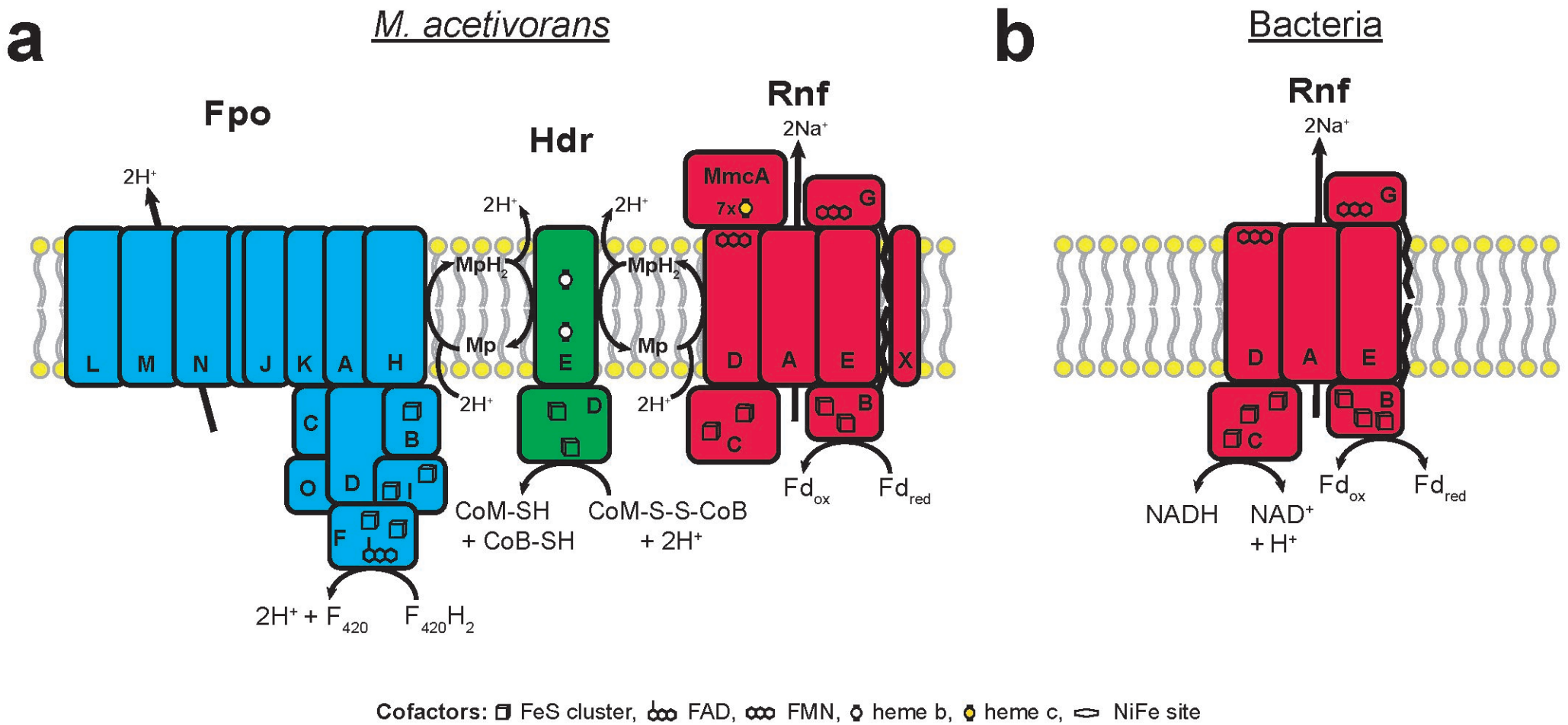

Cofactors: FeS cluster, FAD, FMN, heme b, heme c, NiFe site

Figure 1. a) Schematic of the electron transport chain in *Methanosarcina acetivorans* depicting energy conservation facilitated by two respiratory complexes: 1) the F_{420} dehydrogenase complex in (Fpo) in blue and the *Rhodobacter* nitrogen fixation complex (Rnf) in red along with the terminal electron accepting complex HdrDE in green. **b)** Model of the six-subunit Rnf complex from the bacterium, *Acetobacterium woodii*, which serves as a reversible Na+-pumping Ferredoxin (Fd):NAD+ oxidoreductase (20). Note: the Rnf complex found in members of the *Methanosarcinales* couples the transfer of electrons between the cytosolic Fd pool and the membrane-bound MP pool to sodium translocation. The exact pathway of electron flow from Fd to MP is unknown. Additionally, in the *Methanosarcinales*, Rnf contains eight subunits instead of six, one of which is a multiheme *c*-type cytochrome, MmcA.

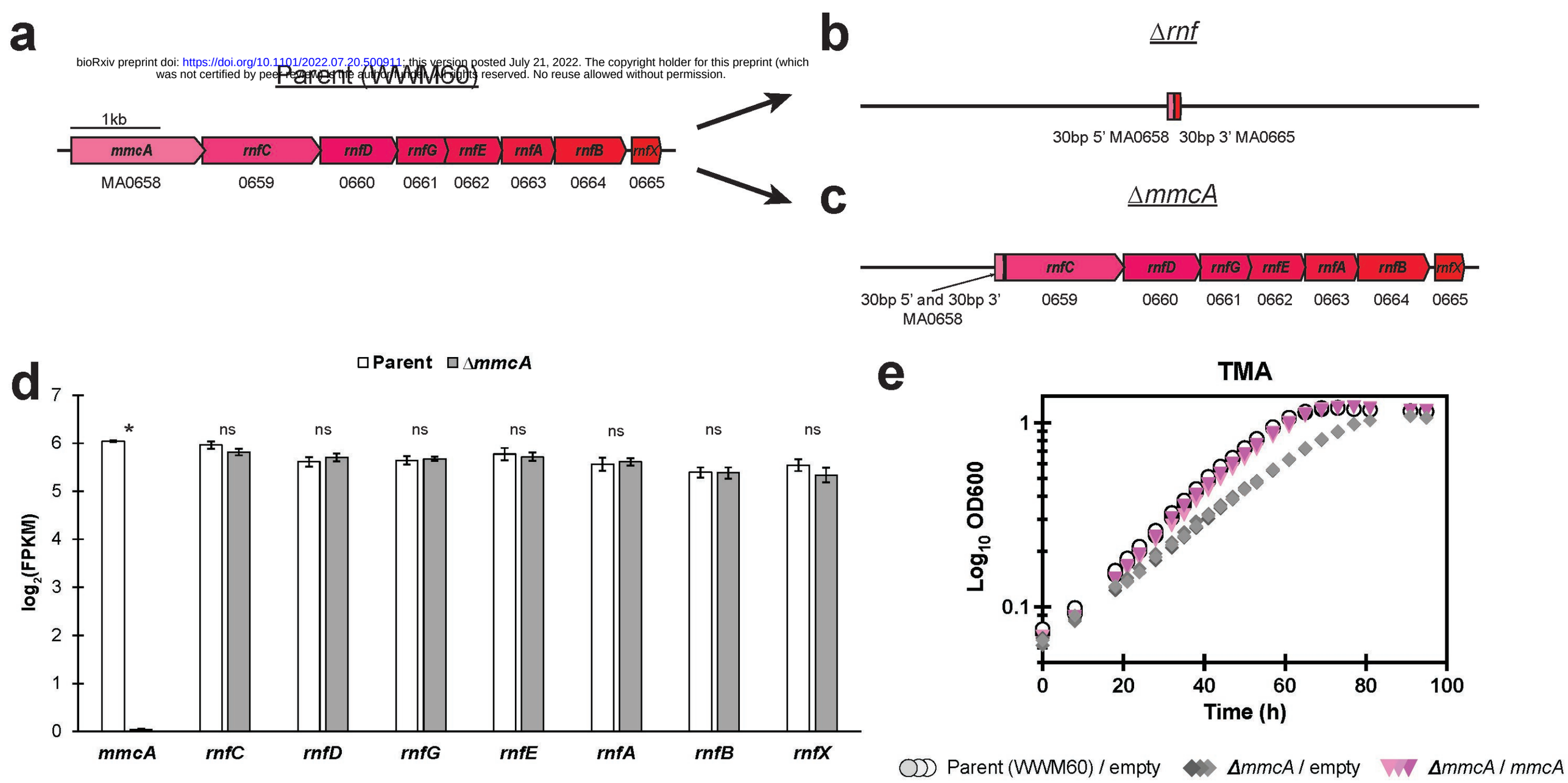

Figure 2. a) Chromosomal organization of the eight-gene *rnf* operon in *M. acetivorans*, reflecting the genotype of the parent strain (WWM60) used in this study. Locus tags are provided under each gene. **b)** Chromosomal organization the *rnf* locus in the Δ*rnf* mutant showing a clean deletion of the operon. A 30 basepair (bp) region of the 5' end of *mmcA* and a 30 bp region of at the 3' end of *rnfX* are maintained on the chromosome to preclude interference with up- and down-stream regulatory elements outside of the operon. **c)** Chromosomal organization of the *rnf* locus in the in the Δ*mmcA* mutant. Here, 30 bp regions at the 5' and 3' ends of *mmcA* are maintained to prevent frameshift disruption of downstream *rnf* genes. **d)** Expression values for the *rnf* genes in the parent and Δ*mmcA* strains. Expression is measured in $\log_2$(FPKM) [fragments per kilobase of transcript per million mapped reads] for each gene. In the Δ*mmcA* strain, only *mmcA* expression is abolished [p-value = 3.5E-9; Welch's t-test] indicating the deletion does not adversely impact on the expression of other genes in the operon. Significance (p-values < 0.05) for $\log_2$(FPKM) values of individual genes between strains is indicated with an asterisk or "ns" for non-significant change. **e)** Growth curve of the parent strain carrying an empty vector control (light gray circles), the Δ*mmcA* mutant carrying an empty vector control (dark gray diamonds), and the Δ*mmcA* mutant carrying a plasmid expressing *mmcA* (pink inverted triangles) in HS medium containing 50 mM TMA as the sole carbon and energy source. The empty vector contains the β-glucoronidase gene, *uidA*, under the control of a tetracycline inducible P*mcrB* (*tetO4*) promoter described previously in (60). The complementation vector contains *mmcA* under the control of a tetracycline indicuble P*mcrB* (*tetO4*) promoter described previously in (24). Three replicate tubes of each strain were used for growth assays and tetracycline was added to a final concentration of 100 ug/mL in the growth medium.

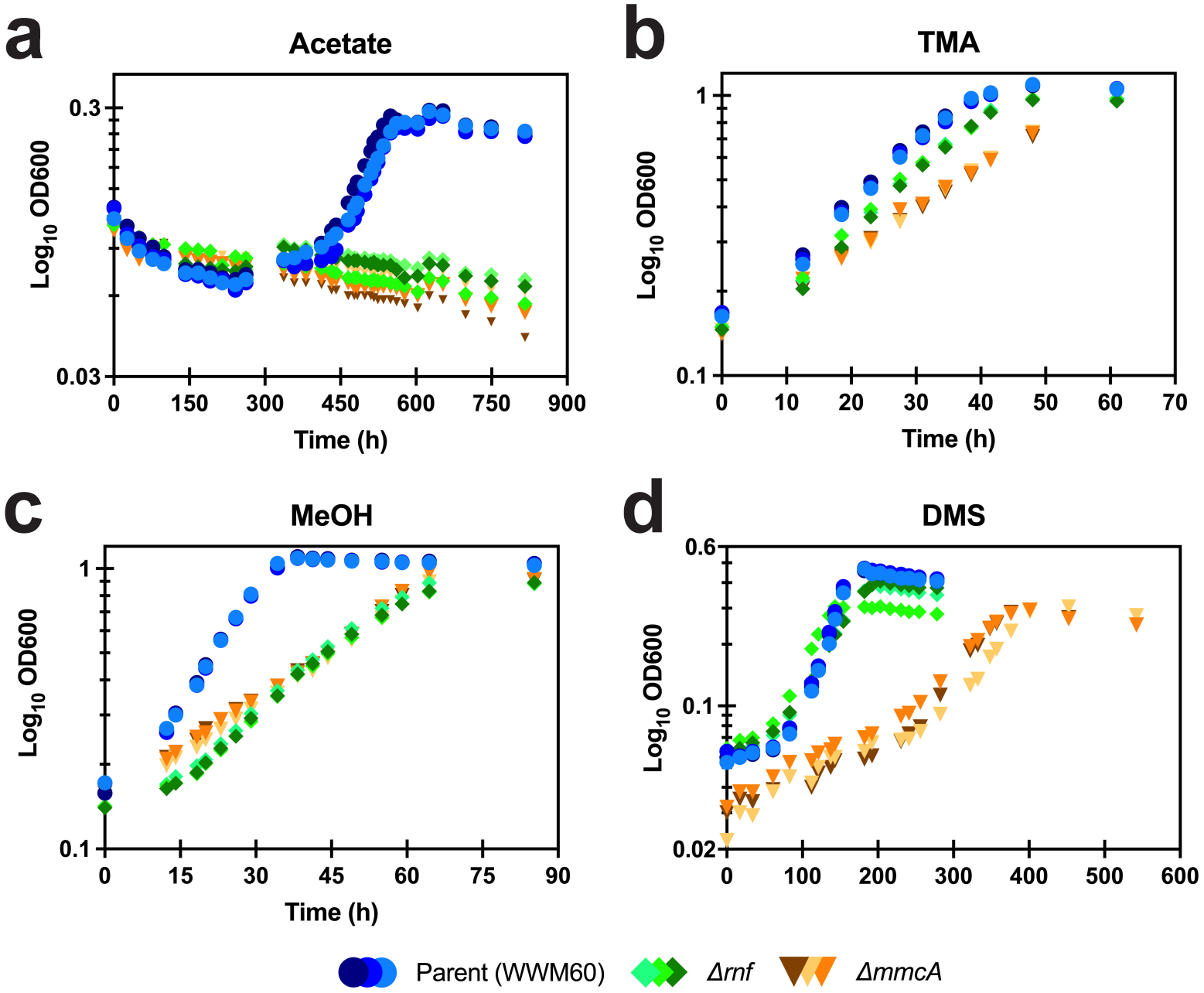

Figure 3. Growth curves of the parent strain (WWM60) (blue circles), Δ*rnf* (green diamonds), and Δ*mmcA* (orange inverted triangles) mutants on **a)** 40 mM acetate, **b)** 50 mM trimethylamine (TMA), **c)** 125 mM methanol (MeOH), and **d)** 20 mM dimethylsulfide (DMS) as the sole carbon and energy source. Three replicate tubes of each strain were used for growth assays.

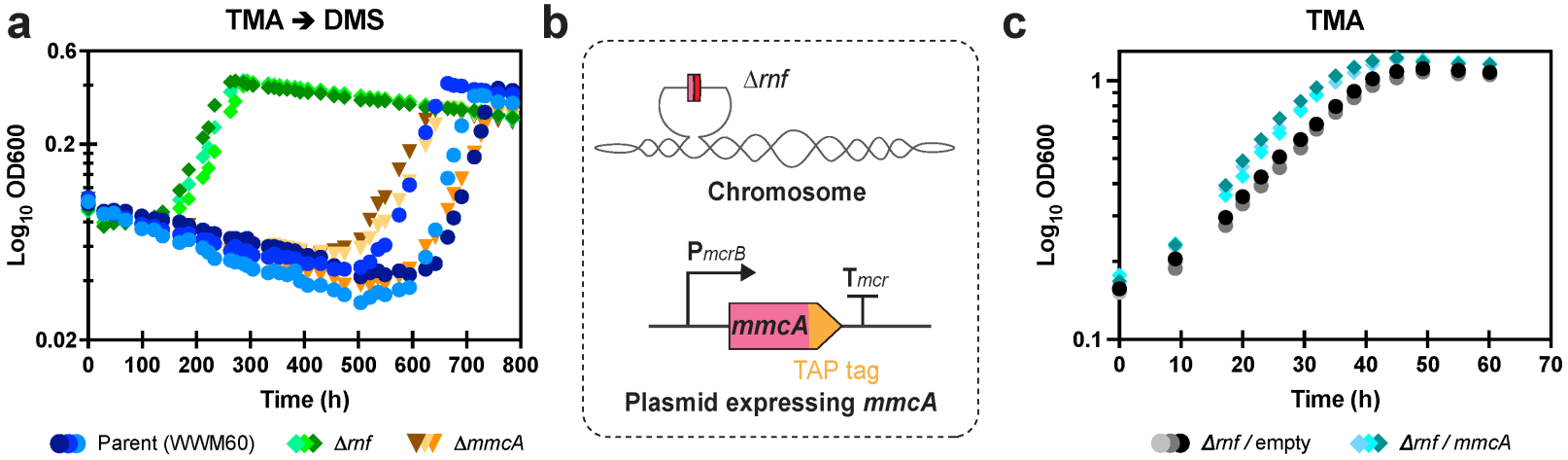

Figure 4. a) Growth curve of the parent strain (WWM60) (blue circles), Δ*rnf* (green diamonds), and Δ*mmcA* (orange inverted triangles) mutants in HS medium containing 20 mM DMS as the sole carbon and energy source after transfer from HS medium with 50 mM TMA as the sole carbon and energy source. **b)** A schematic depicting the genotype of a strain generated to assay the role of *mmcA* in the absence of the rest of the *rnf* genes. On the chromosome, the entire *rnf* locus has been deleted. The strain carries an autonomously replicating plasmid encoding *mmcA* with a tandem-affinity-purification (TAP) tag at the C-terminus under the control of a P*mcrB* promoter described previously in (60). **c)** Growth curve of the Δ*rnf* strain carrying an empty vector control (dark gray circles) or a plasmid expressing *mmcA* (light blue diamonds) in HS medium containing 50 mM TMA as the sole carbon and energy source. The empty vector contains the β-glucoronidase gene, *uidA*, under the control of a PmcrB promoter described previously in (60). Three replicate tubes of each strain were used for growth assays.

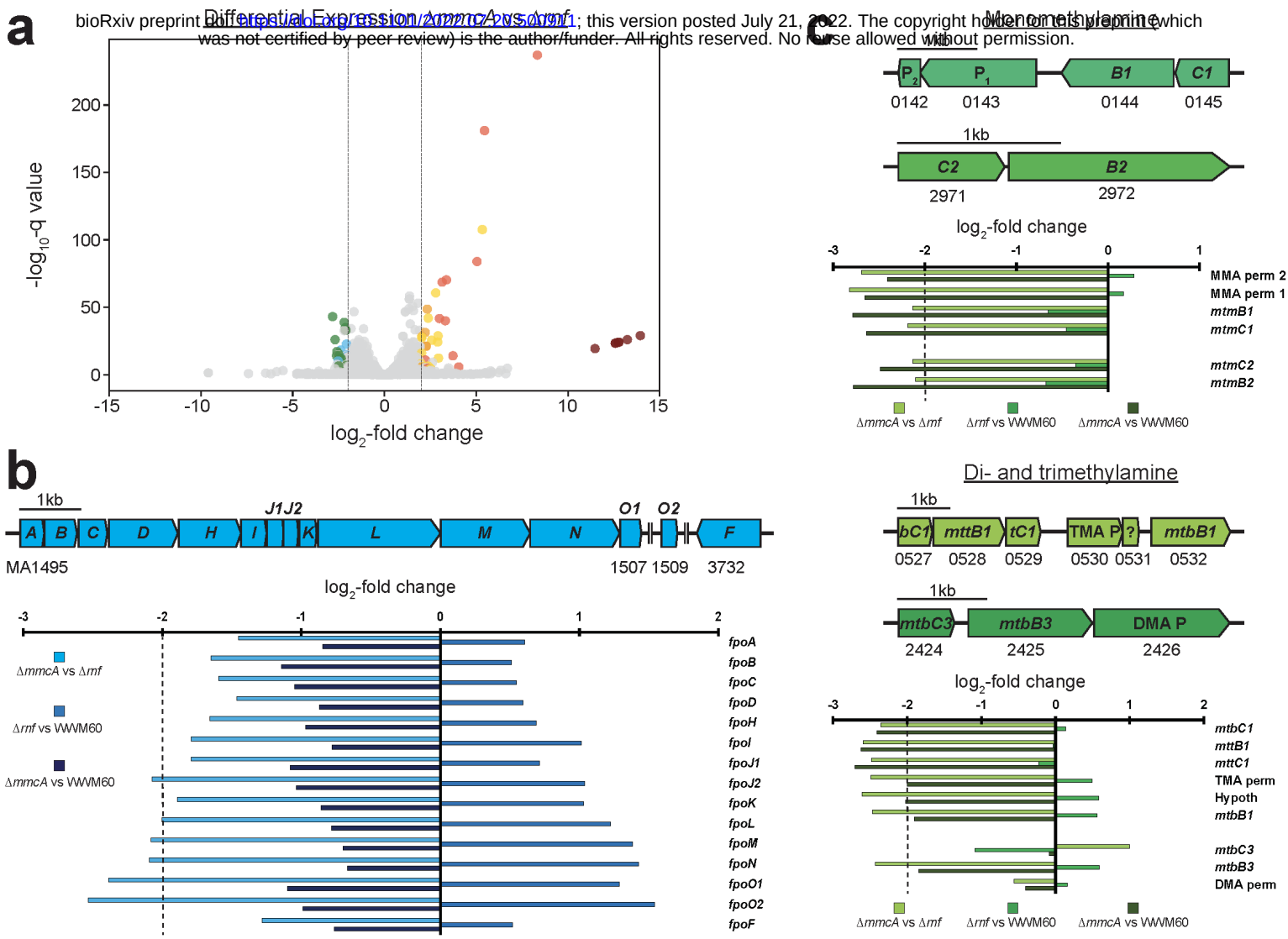

Figure 5. a) Volcano plot showing the differential expression of genes between the Δ*mmcA* and Δ*rnf* mutants. Genes with higher expression in the Δ*mmcA* mutant have a positive $\log_2$-fold change value, while genes with higher expression in the Δ*rnf* mutant have a negative $\log_2$-fold change value. Dashed lines on the plot delineate the cutoff for 'significant' $\log_2$-fold change in transcript abundance in either mutant. In the Δ*rnf* mutant, two sets of genes are significantly more highly expressed: six subunits of the Fpo complex (shaded in blue), and multiple methylamine methyltransferases and permeases (shaded in green). Genes in orange have higher transcript levels in the Δ*mmcA* mutant relative to both the Δ*rnf* mutant and the parent strain (WWM60), genes in gold have significantly lower transcript levels in the Δ*rnf* mutant relative to both the Δ*mmcA* mutant and WWM60, whereas genes in red are uniquely upregulated in the Δ*mmcA* mutant compared to the Δ*rnf* mutant. The seven remaining genes of the Rnf complex in the Δ*mmcA* mutant are shaded in maroon. **b)** Chromosomal organization of the thirteen-gene *fpo* operon in *M. acetivorans*, and the additional *fpoO2* and *fpoF* genes. Double vertical lines indicate genes are located more than 3 kbp away in the genome. The $\log_2$-fold change in transcript abundance for each gene in the Fpo complex for all pairwise comparisons between the Δ*mmcA* mutant, the Δ*rnf* mutant, and WWM60 are shown in the bar graph. The dashed line on the plot delineates the cutoff for 'significant' $\log_2$-fold change in transcript abundance. In the bar graph: light blue bars represent the expression in the Δ*mmcA* mutant compared to the Δ*rnf* mutant, with higher expression in the Δ*mmcA* mutant denoted by a positive $\log_2$-fold change. Medium blue bars represent the expression in the Δ*rnf* mutant compared to the parent strain, with higher expression in the Δ*rnf* mutant denoted by a positive $\log_2$-fold change. Dark blue bars represent the expression in the Δ*mmcA* mutant compared to the parent strain, with higher expression in the Δ*mmcA* strain denoted by a positive $\log_2$-fold change. **c)** Chromosomal organization of four different methylamine methyltransferase loci. The $\log_2$-fold change in transcript abundance for each gene at the various loci for all pairwise comparisons between the Δ*mmcA* mutant, the Δ*rnf* mutant, and WWM60 are shown in the bar graphs. The dashed lines on the plots delineate the cutoff for 'significant' $\log_2$-fold change in transcript abundance. In both bar graphs: light green bars represent the expression in the Δ*mmcA* mutant compared to the Δ*rnf* mutant, with higher expression in the Δ*mmcA* mutant denoted by a positive $\log_2$-fold change. Medium green bars represent the expression in the Δ*rnf* mutant compared to the parent strain, with higher expression in the Δ*rnf* mutant denoted by a positive $\log_2$-fold change. Dark green bars represent the expression in the Δ*mmcA* mutant compared to the parent strain, with higher expression in the Δ*mmcA* strain denoted by a positive $\log_2$-fold change.

Figure 6. a) Volcano plot showing the differential expression of genes between the Δ*rnf* and the parent strain (WWM60). Genes with higher expression in the Δ*rnf* mutant have a positive log_2-fold change value, while genes with higher expression in the parent have a negative log_2-fold change value. Dashed lines on the plot delineate the cutoff for 'significant' log_2-fold change in transcript abundance in either strain. Genes in light purple are significantly differentially expressed in both the Δ*rnf* and Δ*mmcA* mutant relative to the WWM60. Genes in dark magenta have significant differential expression only in the Δ*rnf* mutant relative to WWM60. **b)** Volcano plot showing the differential expression of genes between the Δ*mmcA* and the parent strain (WWM60). Genes with higher expression in the Δ*mmcA* mutant have a positive log_2-fold change value, while genes with higher expression in the parent have a negative log_2-fold change value. Dashed lines on the plot delineate the cutoff for 'significant' log_2-fold change in transcript abundance in either strain. Genes in light purple are significantly differentially expressed in both the Δ*rnf* and Δ*mmcA* mutant relative to the parent strain. Genes in dark purple have significant differential expression only in the Δ*mmcA* mutant relative to the parent. **c)** Schematic of the Na^+-translocating F1F0 ATP synthase in *M. acetivorans*. ATP hydrolysis results in the translocation of three sodium ions across the cell membrane to maintain the sodium gradient in the absence of a fully functional Rnf complex (44). Subunits with significant fold change are shaded in orange. The log_2-fold change in transcript abundance for every gene in the F1F0 ATP synthase between the Δ*rnf* mutant (black bars) and the Δ*mmcA* mutant (gray bars) compared to WWM60 are shown in the bar graph. The dashed line on the plot delineates the cutoff for a 'significant' log_2-fold change in transcript abundance. **d)** Chromosomal organization of the *cdh1* operon in *M. acetivorans*. The log_2-fold change in transcript abundance for each gene in the *cdh1* operon between the Δ*rnf* mutant (black bars) and the Δ*mmcA* mutant (gray bars) compared to WWM60 are shown in the bar graph. The dashed line on the plot delineates the cutoff for a 'significant' log_2-fold change in transcript abundance.

Table 1: Growth data for WWM60, WWM1015 (Δ*rnf*) and DDN009 (Δ*mmcA*) on a range of different methanogenic substrates

M. acetivorans strains	Doubling time (Td) (hrs)	Max.OD_{600} (OD^{M})	p-value for WT vs Δ*rnf* mutant (Td/OD^{M})	p-value for WT vs Δ*mmcA* mutant (Td/OD^{M})	p-value for Δ*rnf* vs Δ*mmcA* mutant (Td/OD^{M})
50 mM Trimethylamine (TMA) as a growth substrate					
WWM60 (WT)	14.94 ± 0.61	1.698	0.043/0.035	0.001/0.355	0.009/0.063
Δ*rnf*	16.72 ± 0.86	1.485	-	-	-
Δ*mmcA*	20.07 ± 0.40	1.632	-	-	-
125 mM Methanol (MeOH) as a growth substrate					
WWM60 (WT)	10.33 ± 0.23	1.899	8.7616E-06/0.001	9.0135E-06/0.002	0.001/0.783
Δ*rnf*	18.58 ± 0.11	1.558	-	-	-
Δ*mmcA*	25.09 ± 0.36	1.569	-	-	-
40 mM Acetate as a growth substrate					
WWM60 (WT)	79.48 ± 5.73	-	-	-	-
Δ*rnf*	No growth	-	-	-	-
Δ*mmcA*	No growth	-	-	-	-
20 mM Dimethyl sulfide (DMS) as a growth substrate					
WWM60 (WT)	26.48 ± 0.13	-	0.023	0.016	0.057
Δ*rnf*	48.54 ± 5.90	-	-	-	-
Δ*mmcA*	67.14 ± 8.90	-	-	-	-

All data represent the mean ± standard deviation of at least 3 biological replicates

p-values were determined using a two-sided t-test assuming unequal variances

Table 2: Growth data for WWM60, WWM1015 (Δ*rnf*) and DDN009 (Δ*mmcA*) on dimethylsulfide (DMS)

M. acetivorans strains	Doubling time (Td) (hrs)	Lag time (hrs)	p-value for WT vs Δ*rnf* mutant (lag time)	p-value for WT vs Δ*mmcA* mutant (lag time)	p-value for Δ*rnf* vs Δ*mmcA* mutant (lag time)
	Growth data for cells transferred from TMA to DMS				
WWM60 (WT)	36.37 ± 4.52	640.60 ± 51.61	0.004	0.367	0.009
Δ*rnf*	53.16 ± 1.92	163.42 ± 13.91	-	-	-
Δ*mmcA*	58.68 ± 5.91	590.22 ± 68.66	-	-	-

All data represent the mean ± standard deviation of at least 3 biological replicates